Novel FDTD Technique Over Tetrahedral Grids for Conductive Media

Lorenzo Codecasa, *Member, IEEE*, Bernard Kapidani, Ruben Specogna, *Member, IEEE*, and Francesco Trevisan

***Abstract*— A fundamental extension for a recently introduced numerical scheme for the time-domain solution of Maxwell's equations on tetrahedral meshes is introduced: the algorithm is here shown to be able to handle materials with finite electric resistivity, without losing any of its amenable properties. A theoretic stability analysis, valid for the extended algorithm, is presented for the first time, and a Courant–Friedrich–Lewy sufficient condition on the maximum time step allowed for the scheme to be stable is derived analytically. This result is completely novel for finite-difference time-domain (FDTD)-like approaches on tetrahedral grids. Finally, the accuracy of the extended algorithm is tested with respect to the well-known implicit finite-element method scheme on tetrahedral grids, to the canonical FDTD scheme on Cartesian orthogonal grids, and to a commercial code implementing FDTD with staircasing mitigation techniques.**

***Index Terms*— Conductive materials, discrete geometric approach (DGA), finite-difference time-domain (FDTD) methods, numerical stability, tetrahedral grids.**

I. Introduction

THE original finite-difference time-domain (FDTD) method, devised by Yee [1], has inspired a conspicuous amount of research in the field of numerical schemes for solving Maxwell's equations in the time domain, thanks to its simplicity and computational efficiency [2]. The original algorithm, which computes the values of electric and magnetic fields on the points of two interlocked Cartesian orthogonal grids, has also been reinterpreted as a finite-integration technique (FIT) algorithm [3], where the computed quantities are the integrals of the field over geometric elements of the grids. Both formulations suffer from the so-called staircase approximation problem: when an interface between regions with discontinuous material properties is not conforming to the Cartesian grid, the second order of accuracy of the finite-difference approximation is lost. In this regard, even recent improved techniques based on combined arithmetic and harmonic averaging techniques [4], [5] do not preserve the original accuracy in the neighborhood of the interface.

This problem is inherent to the Cartesian orthogonal discretization of the domain, as unstructured grids (tetrahedral or polyhedral) mesh generators avoid it with grids conforming to the discontinuities in material properties. Approaches that have had some degree of success in adapting the FDTD algorithm to unstructured grids include schemes based on the finite-element method (FEM) [6]–[8], on the cell method [9]–[13], and more recently, formulations based on the discontinuous Galerkin (DG) approach [16], [17]. Yet, accuracy questions on the DG methods are still open, since these methods do not explicitly require the local fulfillment of physical conservation laws (charge conservation in particular) across mesh element interfaces. On the other hand, classical FEM formulations, which do not share this drawback, can be made unconditionally stable [7], at the cost of the resulting scheme being implicit, i.e., the computation includes solving a linear system of algebraic equations at each time step. This severely limits the scalability of the algorithm. Recently, in the framework of the discrete geometric approach (DGA), a technique has been introduced in [13], which yields an explicit, charge preserving, and conditionally stable algorithm on tetrahedral grids, with the limitation of being formulated for strictly dielectric materials. How to overcome this limitation is unfortunately not obvious. This paper is rooted in the formulation of this previous work and aims at addressing this issue. Furthermore, although the properties of the material operators in [13] show that the resulting scheme is conditionally stable, a Courant–Friedrich–Lewy (CFL) condition equivalent to the one of the original FDTD algorithm is not given. This is also dealt with in the following.

The rest of this paper is organized as follows. The discretization of the equations in the lossless case is reintroduced in Section II for the sake of clarity. The extension of the scheme to the case of lossy materials is introduced in Section III, and details on how to render its implementation efficient are given. A CFL condition for the algorithm is analytically derived in Section IV, where the numerical upper bound on the time step for any given tetrahedral grid is also given. Numerical results, which validate the main results claimed in the rest of this paper, are shown and discussed in Section V. In Section VI, conclusions are drawn.

Manuscript received July 21, 2017; revised April 29, 2018; accepted July 22, 2018. Date of publication August 1, 2018; date of current version October 4, 2018. The work of B. Kapidani was supported by the Austrian Science Fund (FWF) under Project SFB 65. *(Corresponding author: Bernard Kapidani.)*

L. Codecasa is with the Dipartimento di Elettronica, Informazione e Bioingegneria, Politecnico di Milano, I-20133 Milan, Italy (e-mail: lorenzo.codecasa@polimi.it).

B. Kapidani is with the Institute for Analysis and Scientific Computing, Technical University of Vienna, 1040 Wien, Austria (e-mail: bernard.kapidani@asc.tuwien.ac.at).

R. Specogna and F. Trevisan are with the Dipartimento Politecnico di Ingegneria ed Architettura, University of Udine, I-33100 Udine, Italy (e-mail: ruben.specogna@uniud.it; francesco.trevisan@uniud.it).

Color versions of one or more of the figures in this paper are available online at http://ieeexplore.ieee.org.

Digital Object Identifier 10.1109/TAP.2018.2862244

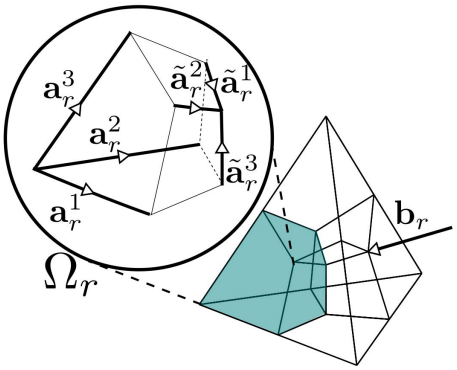

Fig. 1. Hexahedron Ω_r is the element on which the basis functions are defined.

II. Lossless Case Formulation

In the case of materials with infinite resistivity, Maxwell's equations in a bounded finite domain Ω can be written as

$$\frac{\partial \boldsymbol{b}}{\partial t} = -\nabla \times \boldsymbol{e} \tag{1}$$

$$\mu \boldsymbol{h} = \boldsymbol{b} \tag{2}$$

$$\frac{\partial \boldsymbol{d}}{\partial t} = \nabla \times \boldsymbol{h} \tag{3}$$

$$\varepsilon \boldsymbol{e} = \boldsymbol{d} \tag{4}$$

in which μ and ε are symmetric, positive-definite tensors. In the following, we will work in the framework of the DGA, where electromagnetic fields are discretized by taking their integrals, called degrees of freedom (DoFs), over geometric elements of two interlocked meshes: a primal tetrahedral mesh and a polyhedral dual mesh, obtained by the barycentric subdivision of the primal mesh. Discrete differential operators are encoded by the incidence matrices of geometric elements of the mesh, much like it is done in FIT schemes on Cartesian orthogonal grids. Within this framework, the peculiarity of the approach of [13] lies in the choice of the basis functions that discretize constitutive equations. These are discretized locally on every nonempty intersection Ω_r (see Fig. 1) between a tetrahedron τ_v and a dual cell $\tilde{\tau}_{\tilde{v}}$ centered in any of the four vertices of τ_v. The magnetic permeability in (2) is discretized in Ω_r as a 3×3 symmetric, positive-definite matrix $\mathbf{M}_r^{\mu}$, whose entry at its ith row and jth column is

$$\int_{\Omega_r} \tilde{\mathbf{w}}_r^i(\mathbf{r}) \cdot \mu(\mathbf{r}) \tilde{\mathbf{w}}_r^j(\mathbf{r})\, d\mathbf{r} \tag{5}$$

where functions $\tilde{\mathbf{w}}_r^i(\mathbf{r})$ (with $i = 1, 2, 3$) are three constant basis functions with compact support in Ω_r given by

$$\tilde{\mathbf{w}}_r^i(\mathbf{r}) = \frac{\tilde{\mathbf{a}}_r^j \times \tilde{\mathbf{a}}_r^k}{\tilde{\mathbf{a}}_r^i \times \tilde{\mathbf{a}}_r^j \cdot \tilde{\mathbf{a}}_r^k}$$

in which i, j, and k is any permutation of 1, 2, and 3 and $\tilde{\mathbf{a}}_r^1$, $\tilde{\mathbf{a}}_r^2$, and $\tilde{\mathbf{a}}_r^3$ are the tangent vectors of the portions of the three edges of $\tilde{\tau}_{\tilde{v}}$ with nonempty intersection with Ω_r (as shown in Fig. 1). Conversely, the dielectric permittivity tensor of (2) is discretized into a 3×3 symmetric, positive-definite matrix $\mathbf{M}_r^{\varepsilon}$ whose entry at its ith row and jth column is

$$\int_{\Omega_r} \mathbf{w}_r^i(\mathbf{r}) \cdot \varepsilon(\mathbf{r}) \mathbf{w}_r^j(\mathbf{r})\, d\mathbf{r} \tag{6}$$

where functions $\mathbf{w}_r^i(\mathbf{r})$ (with $i = 1, 2, 3$) are three constant basis functions with compact support in Ω_r given by

$$\mathbf{w}_r^i(\mathbf{r}) = \frac{\mathbf{a}_r^j \times \mathbf{a}_r^k}{\mathbf{a}_r^i \times \mathbf{a}_r^j \cdot \mathbf{a}_r^k}$$

in which i, j, and k is any permutation of 1, 2, and 3 and $\mathbf{a}_r^1$, $\mathbf{a}_r^2$, and $\mathbf{a}_r^3$ are the tangent vectors of the portions of the three edges of τ_v with nonempty intersection with Ω_r (as shown in Fig. 1).

Obtaining the discretized version of (2) in global form is straightforwardly done by assembling all the $\mathbf{M}_r^{\mu}$ values contributing to a tetrahedron τ_v and inverting locally the 4×4 resulting matrix. The same can be done locally in every dual cell $\tilde{\tau}_{\tilde{v}}$ for the discrete global version of (4). This yields sparse, symmetric, and positive-definite matrices $\mathbf{M}^{\mu^{-1}}$ and $\mathbf{M}^{\varepsilon^{-1}}$.

With these premises, the discretized Maxwell's equations over a tetrahedral primal grid $\mathcal{G}$ and barycetric dual grid $\tilde{\mathcal{G}}$ are

$$\frac{\boldsymbol{\varphi}^{n+\frac{1}{2}} - \boldsymbol{\varphi}^{n-\frac{1}{2}}}{\Delta t} = -\mathbf{C}\boldsymbol{v}^n \tag{7}$$

$$\tilde{\boldsymbol{f}}^{n+\frac{1}{2}} = \mathbf{M}^{\mu^{-1}} \boldsymbol{\varphi}^{n+\frac{1}{2}} \tag{8}$$

$$\frac{\tilde{\boldsymbol{\psi}}^{n+1} - \tilde{\boldsymbol{\psi}}^{n}}{\Delta t} = \tilde{\mathbf{C}} \tilde{\boldsymbol{f}}^{n+\frac{1}{2}} \tag{9}$$

$$\boldsymbol{v}^{n+1} = \mathbf{M}^{\varepsilon^{-1}} \tilde{\boldsymbol{\psi}}^{n+1} \tag{10}$$

in which the following usual definitions apply: $\boldsymbol{\varphi}^{n+(1/2)}$ is the vector of the fluxes of $\boldsymbol{b}$ through the primal faces of $\mathcal{G}$ at time instant $(n + (1/2))\Delta t$, $\tilde{\boldsymbol{f}}^{n+(1/2)}$ is the vector of line integrals of $\boldsymbol{h}$ along the dual edges of $\mathcal{G}$ at time instant $(n + (1/2))\Delta t$, $\boldsymbol{\psi}^n$ is the vector of the fluxes of $\boldsymbol{d}$ through the dual faces of $\mathcal{G}$ at time instant $n\Delta t$, $\boldsymbol{v}^n$ is the vector of line integrals of $\boldsymbol{e}$ along the primal edges of $\mathcal{G}$ at time instant $n\Delta t$, $\mathbf{C}$ is the primal face-edge incidence matrix of the grid $\mathcal{G}$ and encodes the discrete equivalent of the curl operator, and $\tilde{\mathbf{C}} = \mathbf{C}^T$ is the dual face-edge incidence matrix of the grid $\tilde{\mathcal{G}}$ (^{T} indicating transposition) and again encodes the discrete equivalent of the curl operator. Matrix $\mathbf{M}^{\mu^{-1}}$ transforms the fluxes $\boldsymbol{\varphi}^{n+(1/2)}$ into line integrals $\tilde{\boldsymbol{f}}^{n+(1/2)}$ and ensures the consistency of the discretized equation (8). Matrix $\mathbf{M}^{\varepsilon^{-1}}$ transforms the fluxes $\tilde{\boldsymbol{\psi}}^n$ into line integrals $\boldsymbol{v}^n$ and ensures the consistency of the discretized equation (10). With a few algebraic manipulations, the system of (7) through (10) can be written as

$$\tilde{\boldsymbol{f}}^{n+\frac{1}{2}} = \tilde{\boldsymbol{f}}^{n-\frac{1}{2}} - \Delta t \mathbf{M}^{\mu^{-1}} \mathbf{C} \boldsymbol{v}^n \tag{11}$$

$$\boldsymbol{v}^{n+1} = \boldsymbol{v}^n + \Delta t \mathbf{M}^{\varepsilon^{-1}} \tilde{\mathbf{C}} \tilde{\boldsymbol{f}}^{n+\frac{1}{2}} \tag{12}$$

which define an explicit leapfrog time-marching scheme. It is important to note that the fields obtained by interpolating the numerical solution with the given basis functions are piecewise-uniform, hence in general discontinuous. This peculiarity distances the method from canonical FEM, in which the basis functions need to comply with more stringent sequence properties [14].

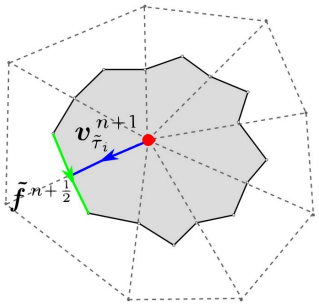

Fig. 2. Local quantities defined on the single dual volume. For the sake of clarity, we show a 2-D section in which the section of the dual volume is the colored area. It is important to note that even if DoFs are defined on dual volumes, material tensors are still piecewise-uniform on primal volumes as in the standard FEM.

III. Introduction of Electric Lossy Materials

In the DGA framework, we want to extend (11) and (12) to the case of lossy materials, without giving up any crucial property of the original FDTD algorithm. Let us first recall that, in the presence of materials with finite resistivity, Ampére–Maxwell's equation in the continuous domain can be written as

$$\varepsilon \frac{\partial \boldsymbol{e}}{\partial t} + \sigma \boldsymbol{e} = \boldsymbol{j}_t \tag{13}$$

$$\boldsymbol{j}_t = \nabla \times \boldsymbol{h} \tag{14}$$

in which $\boldsymbol{j}_t$ is the total electric current density which accounts for both the displacement current term and the ohmic conduction current term. Since (13) contains both $\boldsymbol{e}$ and its derivative, a discretization of (13) and (14) trivially inferred from (7)–(10) would fail in keeping the algorithm explicit. In the following, we show that how this can be achieved with a more subtle approach.

A. Discretization of Ampére–Maxwell Law

Let us consider a single volume $\tilde{\tau}_{\tilde{v}} \in \tilde{\mathcal{G}}$, as in Fig. 2. If we label $\mathcal{F}_{\tilde{\tau}_{\tilde{v}}}$ the set of faces of $\tilde{\mathcal{G}}$ in the boundary of $\tilde{\tau}_{\tilde{v}}$, we can discretize 14) as follows:

$$\tilde{\boldsymbol{i}}_{\tilde{\tau}_{\tilde{v}}}^{n+\frac{1}{2}} = \mathbf{S}_{\tilde{\tau}_{\tilde{v}}} \tilde{\mathbf{C}} \tilde{\boldsymbol{f}}^{n+\frac{1}{2}} \tag{15}$$

where $\tilde{\boldsymbol{i}}_{\tilde{\tau}_{\tilde{v}}}^{n+(1/2)}$ is a column vector of size $|\mathcal{F}_{\tilde{\tau}_{\tilde{v}}}|$, containing the fluxes of $\boldsymbol{j}_t$ through the faces of $\tilde{\mathcal{G}}$ in the boundary of $\tilde{\tau}_{\tilde{v}}$ at time instant $(n+(1/2))\Delta t$, and $\mathbf{S}_{\tilde{\tau}_{\tilde{v}}}$ is a transformation matrix with $|\mathcal{F}_{\tilde{\tau}_{\tilde{v}}}|$ rows and number of columns equal to the number of faces in $\tilde{\mathcal{G}}$. Every row of $\mathbf{S}_{\tilde{\tau}_{\tilde{v}}}$ has exactly one entry equal to 1 corresponding to a dual face in the boundary of $\tilde{\tau}_{\tilde{v}}$ and zero everywhere else. If we then define $\boldsymbol{v}_{\tilde{\tau}_{\tilde{v}}}^n$ as the vector of size $|\mathcal{F}_{\tilde{\tau}_{\tilde{v}}}|$ containing line integrals of $\boldsymbol{e}$ along the *halves* of primal edges of $\mathcal{G}$ which intersect $\tilde{\tau}_{\tilde{v}}$ at time instant $n\Delta t$, (13) can be discretized as follows:

$$\tilde{\boldsymbol{i}}_{\tilde{\tau}_{\tilde{v}}}^{n+\frac{1}{2}} = \mathbf{M}_{\tilde{\tau}_{\tilde{v}}}^{\varepsilon} \frac{\boldsymbol{v}_{\tilde{\tau}_{\tilde{v}}}^{n+1} - \boldsymbol{v}_{\tilde{\tau}_{\tilde{v}}}^{n}}{\Delta t} + \mathbf{M}_{\tilde{\tau}_{\tilde{v}}}^{\sigma} \frac{\boldsymbol{v}_{\tilde{\tau}_{\tilde{v}}}^{n+1} + \boldsymbol{v}_{\tilde{\tau}_{\tilde{v}}}^{n}}{2} \tag{16}$$

where $\mathbf{M}_{\tilde{\tau}_{\tilde{v}}}^{\varepsilon}$ and $\mathbf{M}_{\tilde{\tau}_{\tilde{v}}}^{\sigma}$ are square, symmetric, and positive-definite matrices of size $|\mathcal{F}_{\tilde{\tau}_{\tilde{v}}}|$ discretizing the ε and σ tensors, respectively, and the standard semi-implicit approximation was used for the σ-dependent term on the right-hand side of (16). Matrices $\mathbf{M}_{\tilde{\tau}_{\tilde{v}}}^{\varepsilon}$ and $\mathbf{M}_{\tilde{\tau}_{\tilde{v}}}^{\sigma}$ are constructed *locally on every dual volume*, generalizing to σ the procedure already described for ε in Section II. A remark is in order: for (16), to yield a local consistent discretization of (13) for any $\tilde{\tau}_{\tilde{v}} \in \tilde{\mathcal{G}}$, material tensors ε and σ need not be uniform in the dual volume (they are, in fact, piecewise-uniform on primal volumes as usual). Let us finally define two additional local matrices

$$\mathbf{P}_{\tilde{\tau}_{\tilde{v}}} = \mathbf{M}_{\tilde{\tau}_{\tilde{v}}}^{\varepsilon} + \frac{\Delta t}{2} \mathbf{M}_{\tilde{\tau}_{\tilde{v}}}^{\sigma}$$

$$\mathbf{Q}_{\tilde{\tau}_{\tilde{v}}} = \mathbf{M}_{\tilde{\tau}_{\tilde{v}}}^{\varepsilon} - \frac{\Delta t}{2} \mathbf{M}_{\tilde{\tau}_{\tilde{v}}}^{\sigma}.$$

With these definitions, we can apply a local matrix inversion approach for each $\tilde{\tau}_{\tilde{v}}$: by equating the right-hand sides of (15) and (16) and inverting with respect to $\boldsymbol{v}_{\tilde{\tau}_{\tilde{v}}}^{n+1}$, it ensues

$$\boldsymbol{v}_{\tilde{\tau}_{\tilde{v}}}^{n+1} = (\mathbf{P}_{\tilde{\tau}_{\tilde{v}}})^{-1} \cdot \left(\mathbf{Q}_{\tilde{\tau}_{\tilde{v}}} \boldsymbol{v}_{\tilde{\tau}_{\tilde{v}}}^{n} + \Delta t \mathbf{S}_{\tilde{\tau}_{\tilde{v}}} \tilde{\mathbf{C}} \tilde{\boldsymbol{f}}^{n+\frac{1}{2}} \right) \quad \forall \tilde{\tau}_{\tilde{v}}.$$

It is easy to notice that we can append all local vectors $\boldsymbol{v}_{\tilde{\tau}_{\tilde{v}}}^n$ to form a single global column vector $\boldsymbol{v}_{\tilde{\tau}}^n$. It then ensues

$$\boldsymbol{v}_{\tilde{\tau}}^{n+1} = (\mathbf{P}_{\tilde{\tau}})^{-1} \cdot \left(\mathbf{Q}_{\tilde{\tau}} \boldsymbol{v}_{\tilde{\tau}}^{n} + \Delta t \mathbf{S}_{\tilde{\tau}} \tilde{\mathbf{C}} \tilde{\boldsymbol{f}}^{n+\frac{1}{2}} \right) \tag{17}$$

where $(\mathbf{P}_{\tilde{\tau}})^{-1}$ and $\mathbf{Q}_{\tilde{\tau}}$ have block diagonal matrix form

$$(\mathbf{P}_{\tilde{\tau}})^{-1} = \begin{bmatrix} (\mathbf{P}_{\tilde{\tau}_1})^{-1} & \mathbf{0} & \cdots & \mathbf{0} \\ \mathbf{0} & (\mathbf{P}_{\tilde{\tau}_2})^{-1} & \cdots & \mathbf{0} \\ \vdots & \vdots & \ddots & \vdots \\ \mathbf{0} & \mathbf{0} & \cdots & (\mathbf{P}_{\tilde{\tau}_{|\tilde{v}|}})^{-1} \end{bmatrix}$$

and $\mathbf{S}_{\tilde{\tau}} = [\mathbf{S}_{\tilde{\tau}_1}^T \ \mathbf{S}_{\tilde{\tau}_2}^T \ \cdots \ \mathbf{S}_{\tilde{\tau}_{|\tilde{v}|}}^T]^T$, where $|\tilde{v}|$ is the total number of volumes in $\tilde{\mathcal{G}}$. Matrix $\mathbf{S}_{\tilde{\tau}}$ has exactly two nonzero entries equal to one in each column, since two halved edges correspond to each edge in the primal mesh $\mathcal{G}$. Discrete Equation (17) can be written as

$$\boldsymbol{v}_{\tilde{\tau}}^{n+1} = \mathbf{A}_{\tilde{\tau}} \boldsymbol{v}_{\tilde{\tau}}^{n} + \Delta t \mathbf{B}_{\tilde{\tau}} \tilde{\mathbf{C}} \tilde{\boldsymbol{f}}^{n+\frac{1}{2}}$$

where $\mathbf{A}_{\tilde{\tau}} = (\mathbf{P}_{\tilde{\tau}})^{-1} \mathbf{Q}_{\tilde{\tau}}$ and $\mathbf{B}_{\tilde{\tau}} = (\mathbf{P}_{\tilde{\tau}})^{-1} \mathbf{S}_{\tilde{\tau}}$. It generalizes (12) to the case of lossy media when only it splits electric field DoFs into halved primal edges, effectively adding one unknown for every primal edge of $\mathcal{G}$.

Finally, to have a fully functioning leapfrog time-marching algorithm, one just needs to add back together the halved edge quantities by left-multiplication with the transpose of the appropriate transformation matrix

$$\boldsymbol{v}^{n+1} = \mathbf{S}_{\tilde{\tau}}^T \boldsymbol{v}_{\tilde{\tau}}^{n+1}. \tag{18}$$

The scheme comprising (11), (17), and (18) inherits all the benefits of the FDTD algorithm for lossy materials on Cartesian grids. It is explicit, conditionally stable, and it has the second-order accuracy in time. At no point in its derivation, the properties of (11) and (12) are lost. Furthermore, matrices $(\mathbf{P}_{\tilde{\tau}})^{-1}$ and $\mathbf{Q}_{\tilde{\tau}}$ are both block diagonal so both their construction and their product with DoFs vectors are performed with limited computational effort. Finally, we note that the updating equation (12) is retrieved if $\sigma = 0$ everywhere in the grid.

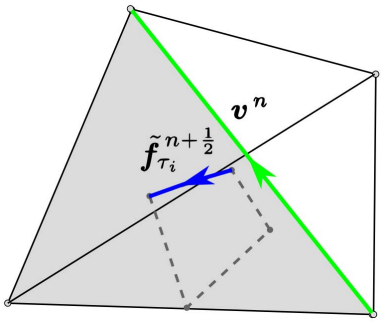

Fig. 3. Local quantities defined on the single tetrahedron.

B. Discretization of Faraday's Law

A similar approach can be applied on the primal mesh. On any single tetrahedron $\tau_v \in \mathcal{G}$, as in Fig. 3, we can discretize (1) on τ_v as follows:

$$\frac{\boldsymbol{\varphi}_{\tau_v}^{n+\frac{1}{2}} - \boldsymbol{\varphi}_{\tau_v}^{n-\frac{1}{2}}}{\Delta t} = -\mathbf{S}_{\tau_v}\mathbf{C}\boldsymbol{v}^n \tag{19}$$

where $\boldsymbol{\varphi}_{\tau_v}^{n+(1/2)}$ is a vector of size 4 containing the fluxes of $\boldsymbol{b}$ through the primal faces of τ_v at time instant $(n+(1/2))\Delta t$. Matrix $\mathbf{S}_{\tau_v}$ is a transformation matrix with four rows and number of columns equal to the number of faces in $\mathcal{G}$. Every row of $\mathbf{S}_{\tau_v}$ has exactly one entry equal to 1 corresponding to a primal face in the boundary of τ_v and zero everywhere else. We can locally construct a symmetric positive-definite 4×4 matrix $(\mathbf{M}_{\tau_v}^{\mu})^{-1}$ that discretizes the μ tensor, with the procedure recalled in Section II, such that the relation

$$\tilde{\boldsymbol{f}}_{\tau_v}^{n+\frac{1}{2}} = \left(\mathbf{M}_{\tau_v}^{\mu}\right)^{-1}\boldsymbol{\varphi}_{\tau_v}^{n+\frac{1}{2}} \tag{20}$$

holds, where $\tilde{\boldsymbol{f}}_{\tau_v}^{n+(1/2)}$ is the vector containing the line integrals of $\boldsymbol{h}$ along the halves of dual edges of $\mathcal{G}$ contained in τ_v, and (20) is a consistent local discretization of (2) for any $\tau_v \in \mathcal{G}$. By substituting (20) into (19) and inverting with respect to $\tilde{\boldsymbol{f}}_{\tau_v}^{n+(1/2)}$, we get

$$\tilde{\boldsymbol{f}}_{\tau_v}^{n+\frac{1}{2}} = \tilde{\boldsymbol{f}}_{\tau_v}^{n-\frac{1}{2}} - \Delta t\left(\mathbf{M}_{\tau_v}^{\mu}\right)^{-1}\mathbf{S}_{\tau_v}\mathbf{C}\boldsymbol{v}^n \quad \forall\tau_v.$$

Let us now define column vector $\tilde{\boldsymbol{f}}_{\tau}^{n+(1/2)}$, obtained by appending all $\tilde{\boldsymbol{f}}_{\tau_v}^{n+(1/2)}$ in $\mathcal{G}$ at time instant $(n+(1/2))\Delta t$. We get

$$\tilde{\boldsymbol{f}}_{\tau}^{n+\frac{1}{2}} = \tilde{\boldsymbol{f}}_{\tau}^{n-\frac{1}{2}} - \Delta t\left(\mathbf{M}_{\tau}^{\mu}\right)^{-1}\mathbf{S}_{\tau}\mathbf{C}\boldsymbol{v}^n \tag{21}$$

where $(\mathbf{M}_{\tau}^{\mu})^{-1}$ has the form

$$(\mathbf{M}_{\tau}^{\mu})^{-1} = \begin{bmatrix} \left(\mathbf{M}_{\tau_1}^{\mu}\right)^{-1} & \mathbf{0} & \cdots & \mathbf{0} \\ \mathbf{0} & (\mathbf{M}_{\tau_2}^{\mu})^{-1} & \cdots & \mathbf{0} \\ \vdots & \vdots & \ddots & \vdots \\ \mathbf{0} & \mathbf{0} & \cdots & (\mathbf{M}_{\tau_{|v|}}^{\mu})^{-1} \end{bmatrix}$$

and $\mathbf{S}_{\tau} = [\mathbf{S}_{\tau_1}^T\ \mathbf{S}_{\tau_2}^T \cdots\ \mathbf{S}_{\tau_{|v|}}^T]^T$, where $|v|$ is the total number of tetrahedra in $\mathcal{G}$. Matrix $\mathbf{S}_{\tau}$ has exactly two nonzero entries in each column associated with any primal face which is not in the boundary of $\mathcal{G}$. The columns of $\mathbf{S}_{\tau}$ which map to faces in the boundary of $\mathcal{G}$ on the other hand will have just one nonzero entry, equal to 1. It is evident that (21) contains the same information of (11), but splits the unknown line integrals of $\boldsymbol{h}$ into halved dual edges, adding one unknown for every primal face of $\mathcal{G}$ which is not in the boundary of Ω. To retrieve the full dual edge DoFs, one just needs to add back together the halved quantities by left-multiplication with the transpose of the appropriate selection matrix

$$\tilde{\boldsymbol{f}}^{n+\frac{1}{2}} = \mathbf{S}_{\tau}^T\,\tilde{\boldsymbol{f}}_{\tau}^{n+\frac{1}{2}}. \tag{22}$$

We remark that, by left-multiplying (21) by $\mathbf{S}_{\tau}^T$ and using (22) recursively, one gets

$$\begin{aligned}\tilde{\boldsymbol{f}}^{n+\frac{1}{2}} &= \mathbf{S}_{\tau}^T\,\tilde{\boldsymbol{f}}_{\tau}^{n+\frac{1}{2}} \\ &= \mathbf{S}_{\tau}^T\,\tilde{\boldsymbol{f}}_{\tau}^{n-\frac{1}{2}} - \Delta t\mathbf{S}_{\tau}^T\mathbf{M}_{\tau}^{\mu^{-1}}\mathbf{S}_{\tau}\mathbf{C}\boldsymbol{v}^n \\ &= \tilde{\boldsymbol{f}}^{n-\frac{1}{2}} - \Delta t\mathbf{M}^{\mu^{-1}}\mathbf{C}\boldsymbol{v}^n\end{aligned}$$

where we have used the fact that $\mathbf{M}^{\mu^{-1}} = \mathbf{S}_{\tau}^T(\mathbf{M}_{\tau}^{\mu})^{-1}\mathbf{S}_{\tau}$ by construction. The additional unknowns for the magnetic field line integrals are, in fact, actually never used in the algorithm. Nevertheless, we introduce them to complete the symmetry of the equations (which can be exploited should a magnetic conductivity need to be introduced, e.g., for PML), and they will be useful in Section IV for the stability analysis.

C. Reduction of Redundant Unknowns

A noticeable drawback of the scheme of (17) and (18) is that it has twice the number of edge unknowns with respect to the actual grid size of Ω. This drawback can be mitigated with algebraic manipulations and with certain, physically relevant, assumptions on the materials' properties.

Let us now take, without loss of generality, a dual volume $\tilde{\tau}_{\tilde{v}}$ contained in a spatial region in which ε and σ are homogenous scalars, and it is straightforward to see from (6) that

$$(\mathbf{P}_{\tilde{\tau}_{\tilde{v}}})^{-1}\cdot\mathbf{Q}_{\tilde{\tau}_{\tilde{v}}} = \frac{\varepsilon - \frac{\Delta t}{2}\sigma}{\varepsilon + \frac{\Delta t}{2}\sigma}\mathbf{I} = \alpha_{\varepsilon,\sigma}\mathbf{I} \tag{23}$$

where $\mathbf{I}$ is the identity matrix and $\alpha_{\varepsilon,\sigma}$ is a dimensionless scalar parameter. This can be done for all edges, which share property (23). The ensuing recombination of halved edges is made clear graphically in Fig. 4: in a shelllike layer of edges (the ones which intersect the annulus bounded by the two dashed lines), the halved primal dual edges must be used, while in the rest of the computational domain, the number of primal edge unknowns is, instead, equal to the number of primal edges in the grid. Formally, this procedure leads to the definition of new hybrid DoFs $\boldsymbol{v}_{\tilde{\rho}}$, such that $\boldsymbol{v}_{\tilde{\rho}} = \mathbf{S}_{\tilde{\rho}\tilde{\tau}}^T\boldsymbol{v}_{\tilde{\tau}}$, where $\mathbf{S}_{\tilde{\rho}\tilde{\tau}}$ is a new transformation matrix, mapping the new DoFs to the ones defined by $\boldsymbol{v}_{\tilde{\tau}}$. Every row of $\mathbf{S}_{\tilde{\rho}\tilde{\tau}}$ is all zeros except for one entry equal to 1, while every column of $\mathbf{S}_{\tilde{\rho}\tilde{\tau}}$ has two or one nonzero coefficients, depending on whether a halved edge lies in a dual volume which shares property (23) or not.

With this formalism, (17) becomes

$$\boldsymbol{v}_{\tilde{\rho}}^{n+1} = \mathbf{A}_{\tilde{\rho}}\boldsymbol{v}_{\tilde{\rho}}^{n} + \Delta t\mathbf{B}_{\tilde{\rho}}\tilde{\mathbf{C}}\tilde{\boldsymbol{f}}^{n+\frac{1}{2}}$$

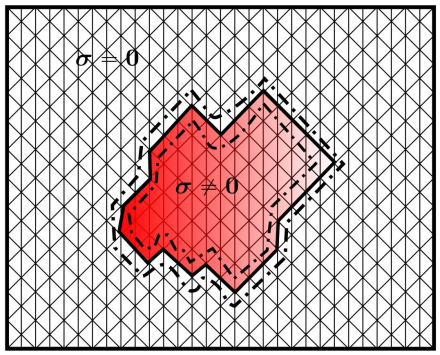

Fig. 4. 2-D section of an example in which the computational domain is split into three regions where the three subcases of the time-marching algorithm apply: the domain Ω is the union of an arbitrarily shaped object Ω_C (the red area in the online version) with $\sigma \neq 0 \in \Omega_C$ and a perfectly dielectric (possibly inhomogenous) region Ω_D given by its complement with respect to a larger box.

where

$$\mathbf{A}_{\tilde{\rho}} = \mathbf{S}^T_{\tilde{\rho}\tilde{\tau}}(\mathbf{P}_{\tilde{\tau}})^{-1}\mathbf{Q}_{\tilde{\tau}}\mathbf{S}_{\tilde{\rho}\tilde{\tau}}\left(\mathbf{S}^T_{\tilde{\rho}\tilde{\tau}}\mathbf{S}_{\tilde{\rho}\tilde{\tau}}\right)^{-1}$$
$$\mathbf{B}_{\tilde{\rho}} = \mathbf{S}^T_{\tilde{\rho}\tilde{\tau}}(\mathbf{P}_{\tilde{\tau}})^{-1}\mathbf{S}_{\tilde{\tau}}$$

and (18) becomes

$$\boldsymbol{v}^{n+1} = \mathbf{S}^T_{\tilde{\tau}}\mathbf{S}_{\tilde{\rho}\tilde{\tau}}\left(\mathbf{S}^T_{\tilde{\rho}\tilde{\tau}}\mathbf{S}_{\tilde{\rho}\tilde{\tau}}\right)^{-1}\boldsymbol{v}^{n+1}_{\tilde{\rho}}$$

where we do not have to actually compute any further matrix inversion, since $\mathbf{S}^T_{\tilde{\rho}\tilde{\tau}}\mathbf{S}_{\tilde{\rho}\tilde{\tau}}$ is a diagonal matrix with all diagonal entries equal to 1 or 2.

In the limit, in which ε and σ are homogenous scalars in the whole grid $\mathcal{G}$, the number of unknowns is reduced to the one given by the original grid. In fact, the procedure yields equations which are equivalent to the starting ones. Algebraic manipulations are just used to merge unknowns associated with line integrals of the electric field in regions of uniform material properties, with no additional assumption on material properties values with respect to the original algorithm. It is also evident from the definitions of $\mathbf{P}$ and $\alpha_{\varepsilon,\sigma}$ that, again, (12) is retrieved if $\sigma = 0$. Finally, it is also relevant to note that the whole procedure of recombination of halved primal edges can be exploited even if instead of homogenous scalars, ε and σ are just proportional tensors.

IV. Stability Analysis

A. Courant–Friedrich–Lewy Condition for the New Algorithm

In the framework introduced in Section III, a stability condition for the resulting algorithm can be derived using considerations formally similar to those used for the FDTD algorithm on Cartesian grids. The algorithm outlined in Section III can be rewritten in the following form:

$$\mathbf{M}^{\mu}_{\tau}\frac{\tilde{\boldsymbol{f}}^{n+\frac{1}{2}}_{\tau} - \tilde{\boldsymbol{f}}^{n-\frac{1}{2}}_{\tau}}{\Delta t} = -\mathbf{S}_{\tau}\,\mathbf{C}\,\mathbf{S}^T_{\tilde{\tau}}\boldsymbol{v}^n_{\tilde{\tau}} \quad (24)$$

$$\mathbf{M}^{\varepsilon}_{\tilde{\tau}}\frac{\boldsymbol{v}^{n+1}_{\tilde{\tau}} - \boldsymbol{v}^n_{\tilde{\tau}}}{\Delta t} + \mathbf{M}^{\sigma}_{\tilde{\tau}}\frac{\boldsymbol{v}^{n+1}_{\tau} + \boldsymbol{v}^n_{\tilde{\tau}}}{2} = \mathbf{S}_{\tilde{\tau}}\,\tilde{\mathbf{C}}\,\mathbf{S}^T_{\tau}\tilde{\boldsymbol{f}}^{n+\frac{1}{2}}_{\tau} \quad (25)$$

where it is also straightforward to see that, if we define $\mathbf{C}_{\tau} = \mathbf{S}_{\tau}\,\mathbf{C}\,\mathbf{S}^T_{\tilde{\tau}}$, it ensues

$$(\mathbf{C}_{\tau})^T = \tilde{\mathbf{C}}_{\tau} = \mathbf{S}_{\tilde{\tau}}\,\tilde{\mathbf{C}}\,\mathbf{S}^T_{\tau}.$$

Then, multiplying on the left (25) by $(\boldsymbol{v}^{n+1}_{\tilde{\tau}} + \boldsymbol{v}^n_{\tilde{\tau}})^T$ and (24) by $(\tilde{\boldsymbol{f}}^{n+(1/2)}_{\tau} + \tilde{\boldsymbol{f}}^{n-(1/2)}_{\tau})^T$ and by summing the two resulting equations and performing a few algebraic manipulations, we obtain

$$W^{n+1} - W^n = -P^{n+\frac{1}{2}} \quad (26)$$

where we have defined

$$W^{n+1} = \frac{1}{2}\left(\boldsymbol{v}^{n+1}_{\tilde{\tau}}\right)^T\mathbf{M}^{\varepsilon}_{\tilde{\tau}}\boldsymbol{v}^{n+1}_{\tilde{\tau}} + \frac{1}{2}\left(\tilde{\boldsymbol{f}}^{n+\frac{1}{2}}_{\tau}\right)^T\mathbf{M}^{\mu}_{\tau}\tilde{\boldsymbol{f}}^{n+\frac{1}{2}}_{\tau} + - \frac{1}{2}\Delta t\left(\boldsymbol{v}^{n+1}_{\tilde{\tau}}\right)^T\tilde{\mathbf{C}}_{\tau}\tilde{\boldsymbol{f}}^{n+\frac{1}{2}}_{\tau} \quad (27)$$

$$W^n = \frac{1}{2}\left(\boldsymbol{v}^n_{\tilde{\tau}}\right)^T\mathbf{M}^{\varepsilon}_{\tilde{\tau}}\boldsymbol{v}^n + \frac{1}{2}\left(\tilde{\boldsymbol{f}}^{n-\frac{1}{2}}_{\tau}\right)^T\mathbf{M}^{\mu}_{\tau}\tilde{\boldsymbol{f}}^{n-\frac{1}{2}}_{\tau} + - \frac{1}{2}\Delta t\left(\boldsymbol{v}^n_{\tilde{\tau}}\right)^T\tilde{\mathbf{C}}_{\tau}\tilde{\boldsymbol{f}}^{n-\frac{1}{2}}_{\tau} \quad (28)$$

$$P^{n+\frac{1}{2}} = \Delta t\left(\frac{\boldsymbol{v}^{n+1}_{\tilde{\tau}} + \boldsymbol{v}^n_{\tilde{\tau}}}{2}\right)^T\mathbf{M}^{\sigma}_{\tilde{\tau}}\left(\frac{\boldsymbol{v}^{n+1}_{\tilde{\tau}} + \boldsymbol{v}^n_{\tilde{\tau}}}{2}\right). \quad (29)$$

By hypothesis on the σ tensor, $P^{n+(1/2)} \geq 0$ always holds. Since (26) also holds, it ensues that the energy function W^n does not increase over time. Consequently, we can use the energy method [18] to establish a CFL condition, i.e., we require $W^n \geq 0$ for each time step. With this approach, we show (see proof in Appendix A) that the following result holds.

Theorem 1: A sufficient condition for the stability of the scheme of Section III is

$$\Delta t < \min_r \frac{h_r}{2c_r}$$

in which the minimum is over all volumes Ω_r (as defined in Section II) in the tetrahedral mesh and h_r is the height of the tetrahedron containing Ω_r, orthogonal to the face opposite to Ω_r.

The condition of Theorem 1 is a theoretical condition which, to the best of our knowledge, is completely novel for the FDTD algorithms on tetrahedral grids, in the sense that it links the time step with a purely geometric property of the mesh and gives a rigorous underpinning to the following intuitive remark: the bound on the stability of a time-domain scheme on tetrahedral grids strongly depends on the quality of the mesh. Tetrahedra which are close to degeneracy (going toward the right in Fig. 5) will be the bottleneck for the conditional stability of the algorithm.

B. Numerical Approach

The approach of Section IV-A yields a sufficient condition for stability, i.e., a theoretic lower bound on Δt. For performance purposes, it may be desirable to obtain the upper bound instead. Using (24), W^{n+1} can be equivalently rewritten as

$$W^{n+1} = \frac{1}{2}\left(\tilde{\boldsymbol{f}}^{n+\frac{1}{2}}_{\tau}\right)^T\mathbf{M}^{\mu}_{\tau}\tilde{\boldsymbol{f}}^{n+\frac{1}{2}}_{\tau} + \frac{1}{2}\left(\boldsymbol{v}^{n+1}_{\tilde{\tau}}\right)^T\mathbf{M}^{\varepsilon}_{\tilde{\tau}}\boldsymbol{v}^n_{\tilde{\tau}} \quad (30)$$

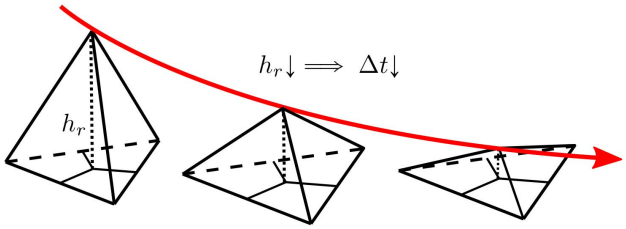

Fig. 5. Grid containing nearly degenerate tetrahedra as the one on the right will require a smaller time step to yield a stable scheme.

and since, again from (24), it is

$$\boldsymbol{v}_{\tilde{\tau}}^{n+1} = \frac{\boldsymbol{v}_{\tilde{\tau}}^{n+1} + \boldsymbol{v}_{\tilde{\tau}}^{n}}{2} + \frac{\Delta t}{2}\left(\mathbf{M}_{\tilde{\tau}}^{\varepsilon}\right)^{-1}\tilde{\mathbf{C}}_{\tau}\,\tilde{\boldsymbol{f}}_{\tau}^{n+\frac{1}{2}}$$
$$\boldsymbol{v}_{\tilde{\tau}}^{n} = \frac{\boldsymbol{v}_{\tilde{\tau}}^{n+1} + \boldsymbol{v}_{\tilde{\tau}}^{n}}{2} - \frac{\Delta t}{2}\left(\mathbf{M}_{\tilde{\tau}}^{\varepsilon}\right)^{-1}\tilde{\mathbf{C}}_{\tau}\,\tilde{\boldsymbol{f}}_{\tau}^{n+\frac{1}{2}}$$

from (30), it then ensues

$$W^{n+1} = \frac{1}{2}\left(\tilde{\boldsymbol{f}}_{\tau}^{n+\frac{1}{2}}\right)^{T}\left(\mathbf{M}_{\tau}^{\mu} - \left(\frac{\Delta t}{2}\right)^{2}\mathbf{C}_{\tau}\left(\mathbf{M}^{\varepsilon}\right)^{-1}\tilde{\mathbf{C}}_{\tau}\right)\tilde{\boldsymbol{f}}_{\tau}^{n+\frac{1}{2}} + \frac{1}{2}\left(\frac{\boldsymbol{v}_{\tilde{\tau}}^{n+1} + \boldsymbol{v}_{\tilde{\tau}}^{n}}{2}\right)^{T}\mathbf{M}_{\tilde{\tau}}^{\varepsilon}\left(\frac{\boldsymbol{v}_{\tilde{\tau}}^{n+1} + \boldsymbol{v}_{\tilde{\tau}}^{n}}{2}\right)$$

from which it results that our numerical scheme is stable if and only if

$$\mathbf{M}_{\tau}^{\mu} - \left(\frac{\Delta t}{2}\right)^{2}\mathbf{C}_{\tau}\left(\mathbf{M}_{\tilde{\tau}}^{\varepsilon}\right)^{-1}\tilde{\mathbf{C}}_{\tau} > 0 \tag{31}$$

where by >0, it is meant that the matrix is positive-definite. We can apply an approach similar to [7] and [19] on (31), obtaining the condition

$$\Delta t < \frac{2}{\sqrt{\lambda_{\mathrm{MAX}}}}$$

where λ_{MAX} is the maximum eigenvalue of matrix $(\mathbf{M}_{\tau}^{\mu})^{-1}\mathbf{C}_{\tau}(\mathbf{M}_{\tilde{\tau}}^{\varepsilon})^{-1}\tilde{\mathbf{C}}_{\tau}$. Since no big matrix inversion needs to be computed, a good estimate of λ_{MAX} can be achieved with the modest computational effort.

V. Numerical Results

A. Uniform Conductive Waveguide

Our first example concerns the simulation of a rectangular metallic waveguide of size 5×2.5 cm and length 10 cm in the z-direction. At $z = 0$, the waveguide is excited with the incident electric field of the TE_{10} modulated with the function $h(t) = \sin(2\pi f t)\Theta(t)$, where $f = 5$ GHz and $\Theta(t)$ is the unit step function. On the other end ($z = 10$ cm), a perfect electric conductor (PEC) termination is applied. We fill the whole waveguide with a medium with nonnegligible electric conductivity σ. A closed form for the solution of this problem, derived in Appendix B, was not previously published to the best of our knowledge. To validate the presented method, comparison with both the analytic solution and other widely known approaches has been performed both for the lossless case and for $\sigma = 50$ mS/m. Using the following energy norm:

$$\|\tilde{\boldsymbol{f}}_{\tau}\|_{\mu} = \frac{1}{2}\left((\tilde{\boldsymbol{f}}_{\tau})^{T}\mathbf{M}_{\tau}^{\mu}\tilde{\boldsymbol{f}}_{\tau}\right)^{\frac{1}{2}}$$
$$\|\boldsymbol{v}_{\tilde{\tau}}\|_{\varepsilon} = \frac{1}{2}\left((\boldsymbol{v}_{\tilde{\tau}})^{T}\mathbf{M}_{\tilde{\tau}}^{\varepsilon}\boldsymbol{v}_{\tilde{\tau}}\right)^{\frac{1}{2}}$$
$$\|\tilde{\boldsymbol{f}}_{\tau}, \boldsymbol{v}_{\tilde{\tau}}\|_{\mu,\varepsilon} = \left(\|\tilde{\boldsymbol{f}}_{\tau}\|_{\mu}^{2} + \|\boldsymbol{v}_{\tilde{\tau}}\|_{\varepsilon}^{2}\right)^{\frac{1}{2}}$$

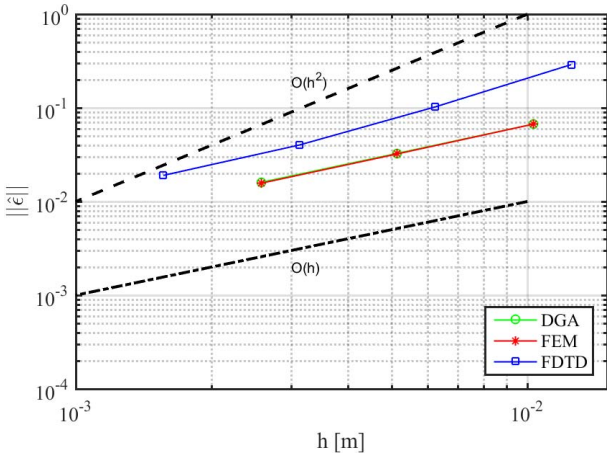

Fig. 6. Relative error in energy norm: $\sigma = 0$ everywhere inside the waveguide (h is the maximum edge length of the mesh element in the grid).

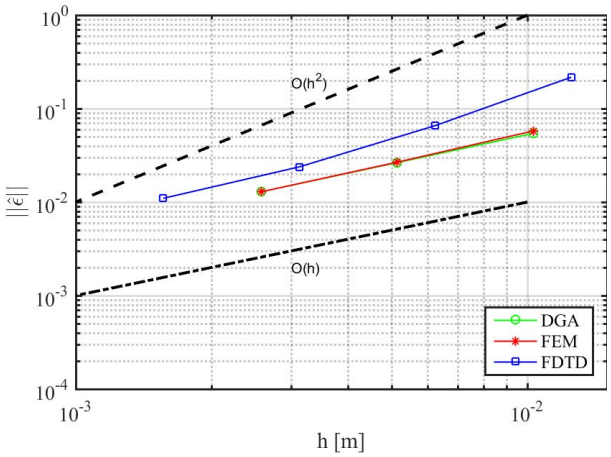

Fig. 7. Relative error in energy norm: $\sigma = 50\ \mathrm{mS \cdot m^{-1}}$ everywhere inside the waveguide (h is the maximum edge length of the mesh element in the grid).

we compared the accuracies of the various methods by studying the relative error

$$\hat{\epsilon} = \frac{\|\tilde{\boldsymbol{f}}_{\tau} - \Pi(\boldsymbol{h}), \boldsymbol{v}_{\tilde{\tau}} - \Pi(\boldsymbol{e})\|_{\mu,\varepsilon}}{\|\Pi(\boldsymbol{h}), \Pi(\boldsymbol{e})\|_{\mu,\varepsilon}}$$

where $\Pi(\boldsymbol{h})$ and $\Pi(\boldsymbol{e})$ are the projections of the analytic fields into the geometric elements of the mesh. Figs. 6 and 7 show the relative error $\hat{\epsilon}$, with respect to the maximum edge length h of the mesh element, in a lossless and lossy waveguide, respectively. The other methods shown are the classical FDTD algorithm (in its FIT variation [3]) and the centered difference discretization of the time-domain FEM approach [7]. The grids used for the FEM and DGA approaches have 14 336, 114 688, 917 504 elements, respectively, and are successive uniform refinements of the same grid. The grids used for the FDTD approach have 4 096, 32 768, 262 144 cubes, respectively. We remark that the FDTD slopes do not show any superconvergent behavior since the fields in the solution of the problem are only piecewise differentiable [20]. The error curves show that the accuracy of the proposed method is in very close agreement with the standard FEM with the lowest order edge elements in both the lossless and the conductive waveguide problems.

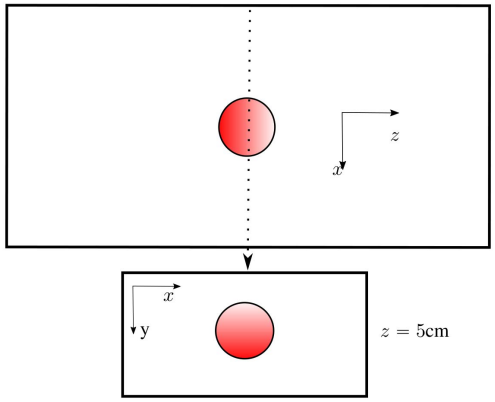

Fig. 8. Two projections of the simulation setup for the numerical example of Section V-B.

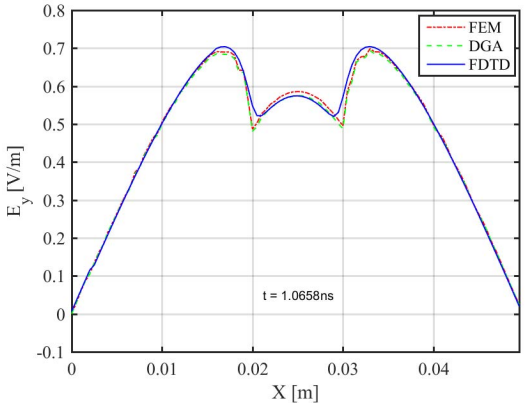

Fig. 9. Comparison of various approaches for the setup of Fig. 8. The tetrahedral grid used comprises 5 402 984 tetrahedra, while the Cartesian orthogonal grid comprises 8 000 000 cubes.

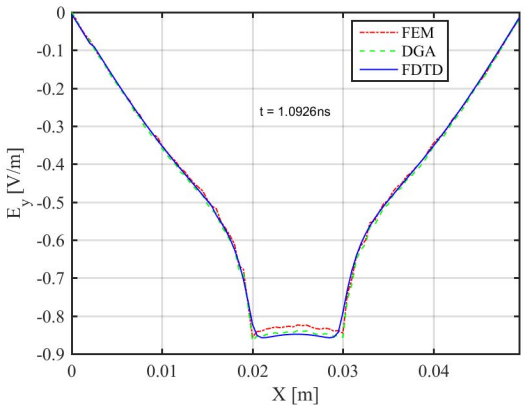

Fig. 10. Comparison of various approaches for the setup of Fig. 8: different time instants.

B. Conductive Ball in Dielectric Waveguide

The second example concerns a dielectric waveguide with the same geometry and excitation, in which a spherical conductive obstacle with radius $r = 5$ mm has been put at the center of the waveguide. We set $\sigma_{\text{ball}} = 0.2\ \text{S} \cdot \text{m}^{-1}$ and $\varepsilon_r = 1$. To illustrate how the various methods behave at the discontinuity between the conductive and dielectric objects, we measured the transverse electric field on a line parallel to the x-axis (setting $z = 0.05$ and $y = 0.0125$). The results for the various approaches are shown at three different instants in Figs. 9 and 10.

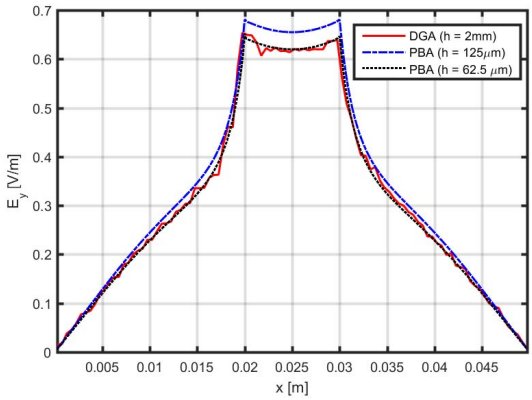

Fig. 11. Comparison with CST MWS commercial code for the setup of Fig. 8: $t = 1.5$ ns.

The analytical solution to this problem is not known, but we can still assess the accuracy of the proposed method as follows: a tetrahedral grid is chosen and the test problem is solved using the FEM approach. Then, the grid is uniformly refined (by bisecting the edges of all tetrahedra), and the problem is solved again. The process is repeated until the energy norm (over the whole domain) of the obtained solution does not vary by more than 1% with respect to the previous refinement. By doing so, we stopped at a grid with 5 402 984 tetrahedra (for a maximum of 17 117 836 unknowns, counting also splits DoFs in the DGA approach). It can be easily noticed that the waveforms obtained with the proposed method (on the same grid) follow closely the ones obtained with the FEM, while the ones obtained with an FDTD simulation with 8 million cubes (48 420 700 unknowns) still show the evident signs of staircasing error in the form of a shift in the discontinuities between air and the conductive material at $x = 0.02$ m and $x = 0.03$ m. To shed some perspective on the performance of the proposed method, it must be noted that simulating 2 ns of propagation with the FEM approach, for which a precoditioned conjugate gradient solver was used, with the tolerance on the relative residual set to 1×10^{-8}, took nearly 30 h, while the simulation with the proposed method (on the same mesh) took approximately 2.5 h on the same architecture.

Finally, in Fig. 11, the same test bench is used to compare the DGA approach to a known commercial code (CST Microwave Studio) implementing closed-source techniques labeled perfect boundary approximation (PBA, see [21]) to avoid staircasing. As a reference, a PBA simulation with a maximum grid step size of 62 μm was used, and the transverse electric field was measured at time instant $t = 1.5$ ns. The plot shows that the DGA approach with maximum grid size of 2 mm (1 million tetrahedra roughly) already shows a very good agreement with the reference solution and is visibly more accurate than a PBA simulation with a grid step $h = 125$ μm (roughly 50 million cubes/hexahedra). The reference solution took roughly 8 h to simulate 2 ns of wave propagation on a Xeon workstation, while the DGA simulation shown in Fig. 11 took less than 10 min on the same workstation. Obviously, the FDTD approach has the clear advantage in terms of number of unknowns for the same grid size and parallel computing performance, but it can be shown (see [15]) that the fractured grid formulation used in this paper allows

the scheme proposed in this paper to achieve an order of magnitude in speedup if implemented on graphic processing units.

VI. Conclusion

An explicit numerical method for the time-domain solution of Maxwell's equations on tetrahedral grids has been described. This method allows to treat materials with arbitrary electric conductivity with limited added computational cost and has been shown analytically to have a CFL condition for numerical stability depending on the geometric properties of the mesh. The method's promise for practical applications has been shown with various numerical tests.

Adaptation of the method to handling open problems is currently under way.

Appendix A
Proof of Theorem 1

To prove Theorem 1, we need the following preliminary lemma.

Lemma 1: For every intersection Ω_r of a dual volume $\tilde{v}$ with a primal volume v, the following identity holds:

$$\mathbf{A}_r \mathbf{M}_r^{\varepsilon} \mathbf{A}_r^T = \varepsilon_r |\Omega_r| \mathbf{I}_3 \tag{32}$$

$$\tilde{\mathbf{A}}_r \mathbf{M}_r^{\mu} \tilde{\mathbf{A}}_r^T = \mu_r |\Omega_r| \mathbf{I}_3 \tag{33}$$

where $\mathbf{I}_3$ is the 3×3 identity matrix, $\mathbf{M}_r^{\mu}$ and $\mathbf{M}_r^{\varepsilon}$ are the 3×3 matrix whose entries are defined in (5) and (6), ε_r is the electric permittivity (assumed uniform in the volume Ω_r), $|\Omega_r|$ indicates the measure of Ω_r, $\mathbf{A}_r = [\mathbf{a}_r^1\ \mathbf{a}_r^2\ \mathbf{a}_r^3]$ is a 3×3 matrix whose columns are the edge vectors of the halves of primal edges on the boundary of Ω_r, and $\tilde{\mathbf{A}}_r = [\tilde{\mathbf{a}}_r^1\ \tilde{\mathbf{a}}_r^2\ \tilde{\mathbf{a}}_r^3]$ is a 3×3 matrix whose columns are the edge vectors of the halves of dual edges on the boundary of Ω_r.

Proof: At any time instant t^n, take a pair of vectors $\boldsymbol{e}_r^n$ and $\boldsymbol{d}_r^n$. We can always define discrete DoFs as projections of uniform vector fields on primal halved edges in the boundary of Ω_r in the following fashion:

$$\boldsymbol{u}_r^n = \mathbf{A}_r^T \boldsymbol{d}_r^n, \quad \boldsymbol{v}_r^n = \mathbf{A}_r^T \boldsymbol{e}_r^n.$$

Then, by using the properties of the basis functions, the following equality holds exactly:

$$\begin{aligned}
&\left(\boldsymbol{d}_r^n\right)^T \mathbf{A}_r \mathbf{M}_r^{\varepsilon} \mathbf{A}_r^T \boldsymbol{e}_r^n \\
&= \left(\boldsymbol{u}_r^n\right)^T \mathbf{M}_r^{\varepsilon} \boldsymbol{v}_r^n \\
&= \sum_{i=1}^{3} \sum_{j=1}^{3} \left(\boldsymbol{u}_r^n\right)_i \left(\int_{\Omega_r} \mathbf{w}_r^i(\mathbf{r}) \cdot \varepsilon(\mathbf{r}) \mathbf{w}_r^j(\mathbf{r})\, d\mathbf{r} \right) \left(\boldsymbol{v}_r^n\right)_j \\
&= \int_{\Omega_r} \sum_{i=1}^{3} \left(\boldsymbol{u}_r^n\right)_i \mathbf{w}_r^i(\mathbf{r}) \cdot \varepsilon(\mathbf{r}) \sum_{j=1}^{3} \left(\boldsymbol{v}_r^n\right)_j \mathbf{w}_r^j(\mathbf{r})\, d\mathbf{r} \\
&= \boldsymbol{d}_r^n \cdot \left(\int_{\Omega_r} \varepsilon(\mathbf{r})\, d\mathbf{r} \right) \boldsymbol{e}_r^n.
\end{aligned}$$

Furthermore, if the electric permittivity is uniform in Ω_r, we get

$$\begin{aligned}
\left(\boldsymbol{d}_r^n\right)^T \mathbf{A}_r \mathbf{M}_r^{\varepsilon} \mathbf{A}_r^T \boldsymbol{e}_r^n &= \boldsymbol{d}_r^n \cdot \left(\int_{\Omega_r} \varepsilon(\mathbf{r})\, d\mathbf{r} \right) \boldsymbol{e}_r^n \\
&= \boldsymbol{d}_r^n \cdot (\varepsilon_r |\Omega_r|) \boldsymbol{e}_r^n.
\end{aligned}$$

Since the choice of vectors $\boldsymbol{d}_r^n$ and $\boldsymbol{e}_r^n$ is general, (32) easily follows. The proof of (33) is completely analogous. □

We are now ready to prove Theorem 1.

Proof: The energy function W^{n+1} in (27) can be rewritten as a sum of terms, one for each volume Ω_r. In fact

$$W^{n+1} = \sum_{r=1}^{4|v|} W_r^{n+1}$$

in which

$$\begin{aligned}
W_r^{n+1} = \frac{1}{2} \left(\boldsymbol{v}_r^{n+1}\right)^T \mathbf{M}_r^{\varepsilon} \boldsymbol{v}_r^{n+1} + \frac{1}{2} \left(\tilde{\boldsymbol{f}}_r^{n+\frac{1}{2}}\right)^T \mathbf{M}_r^{\mu} \tilde{\boldsymbol{f}}_r^{n+\frac{1}{2}} + \\
- \frac{1}{2} \Delta t \left(\boldsymbol{v}_r^{n+1}\right)^T \mathbf{C}_r^T \tilde{\boldsymbol{f}}_r^{n+\frac{1}{2}}.
\end{aligned} \tag{34}$$

Here, quantity W_r^{n+1} is the electromagnetic energy in Ω_r. It is a function of the three-row vector $\boldsymbol{v}_r^{n+1}$, which contains line integrals of the electric field along $\mathbf{a}_r^1$, $\mathbf{a}_r^2$, and $\mathbf{a}_r^3$ and of the three-row vector $\tilde{\boldsymbol{f}}_r^{n+(1/2)}$, which contains line integrals of the magnetic field along $\tilde{\mathbf{a}}_r^1$, $\tilde{\mathbf{a}}_r^2$, and $\tilde{\mathbf{a}}_r^3$ (oriented as shown in Fig. 1). Matrices $\mathbf{M}_r^{\mu}$ and $\mathbf{M}_r^{\varepsilon}$ are the ones defined in (5) and (6), while $\mathbf{C}_r$ is a 3×3 incidence matrix given by

$$\mathbf{C}_r = \begin{bmatrix} 0 & -1 & 1 \\ 1 & 0 & -1 \\ -1 & 1 & 0 \end{bmatrix}.$$

Now, it can be written as

$$\boldsymbol{v}_r^{n+1} = \mathbf{A}_r^T \boldsymbol{e}_r^{n+1} \tag{35}$$

$$\tilde{\boldsymbol{f}}_r^{n+\frac{1}{2}} = \tilde{\mathbf{A}}_r^T \boldsymbol{h}_r^{n+\frac{1}{2}} \tag{36}$$

in which $\boldsymbol{e}_r^{n+1}$ and $\boldsymbol{h}_r^{n+(1/2)}$ are, respectively, the uniform electric and magnetic field vectors in the volume Ω_r, uniquely reconstructed from $\boldsymbol{v}_r^{n+1}$ and $\tilde{\boldsymbol{f}}_r^{n+(1/2)}$.

By substituting (35) and (36) into (34), it ensues

$$\begin{aligned}
2\ W_r^{n+1} = \left(\boldsymbol{e}_r^{n+1}\right)^T \mathbf{A}_r \mathbf{M}_r^{\varepsilon} \mathbf{A}_r^T \boldsymbol{e}_r^{n+1} + \left(\boldsymbol{h}_r^{n+\frac{1}{2}}\right)^T \tilde{\mathbf{A}}_r \mathbf{M}_r^{\mu} \tilde{\mathbf{A}}_r^T \boldsymbol{h}_r^{n+\frac{1}{2}} \\
- \Delta t \left(\boldsymbol{e}_r^{n+1}\right)^T \mathbf{A}_r \mathbf{C}_r^T \tilde{\mathbf{A}}_r^T \boldsymbol{h}_r^{n+\frac{1}{2}}.
\end{aligned}$$

If the dielectric permittivity and the magnetic permeability are uniform scalars, labeled ε_r and μ_r, respectively, in each Ω_r and if we indicate with $|\Omega_r|$ the measure of Ω_r, by Lemma 1, it ensues

$$\frac{2\ W_r^{n+1}}{|\Omega_r|} = \varepsilon_r \left(\boldsymbol{e}_r^{n+1}\right)^2 + \mu_r \left(\boldsymbol{h}_r^{n+\frac{1}{2}}\right)^2 - 2\Delta t\, \boldsymbol{e}_r^{n+1} \times \boldsymbol{h}_r^{n+\frac{1}{2}} \cdot \boldsymbol{u}_r$$

being $\boldsymbol{u}_r = \mathbf{b}_r / (6|\Omega_r|)$, in which $\mathbf{b}_r$ is the face vector of the face of $\mathcal{G}$ opposite to Ω_r, and where we have also used the fact that

$$\left(\boldsymbol{e}_r^{n+1}\right)^T \mathbf{A}_r \mathbf{C}_r^T \tilde{\mathbf{A}}_r^T \boldsymbol{h}_r^{n+\frac{1}{2}} = \frac{1}{3} \boldsymbol{e}_r^{n+1} \times \boldsymbol{h}_r^{n+\frac{1}{2}} \cdot \mathbf{b}_r.$$

Equivalently, it is

$$2 \frac{W_r^{n+1}}{|\Omega_r|} = \left(\boldsymbol{x}_r^{n+\frac{1}{2}}\right)^2 + \left(\boldsymbol{y}_r^{n+1}\right)^2 - 2\Delta t\, c_r \boldsymbol{x}_r^{n+\frac{1}{2}} \times \boldsymbol{y}_r^{n+1} \cdot \boldsymbol{u}_r$$

in which $\boldsymbol{x}_r^{n+(1/2)} = \sqrt{\varepsilon_r} \boldsymbol{e}_r^{n+1}$, $\boldsymbol{y}_r^{n+1} = \sqrt{\mu_r} \boldsymbol{h}_r^{n+(1/2)}$, and $c_r = 1/\sqrt{\varepsilon_r \mu_r}$ is the speed of light in volume Ω_r. Let us now take an arbitrary electromagnetic field $[\boldsymbol{x}^T\ \boldsymbol{y}^T] \neq \mathbf{0}$ in Ω_r.

For $W_r^{n+1} \geq 0$ to hold for every electromagnetic field, we have to require that

$$\begin{aligned} 0 &\leq (\boldsymbol{x})^2 + (\boldsymbol{y})^2 - 2\Delta t\, c_r |\boldsymbol{x}|\,|\boldsymbol{y}|\,|\boldsymbol{u}_r| \\ &= (\boldsymbol{x})^2 + (\boldsymbol{y})^2 - 2|\boldsymbol{x}|\,|\boldsymbol{y}| + 2\,(1 - \Delta t\, c_r\,|\boldsymbol{u}_r|)|\boldsymbol{x}|\,|\boldsymbol{y}| \\ &= (|\boldsymbol{x}| - |\boldsymbol{y}|)^2 + 2\,(1 - \Delta t\, c_r\,|\boldsymbol{u}_r|)|\boldsymbol{x}|\,|\boldsymbol{y}| \end{aligned}$$

from which it ensues that, if we require

$$\Delta t < \frac{1}{c_r |\boldsymbol{u}_r|}$$

it is $W_r^{n+1} \geq 0$ and $W_r^{n+1} = 0$ implies $[\boldsymbol{x}^T\, \boldsymbol{y}^T] = \mathbf{0}$. Thus, observing that $|\boldsymbol{u}_r| = 2/h_r$, in which h_r is the height of the tetrahedron containing Ω_r, normal to the face with face vector $\mathbf{b}_r$, the following condition ensues:

$$\Delta t < \frac{h_r}{2c_r}. \tag{37}$$

Taking the minimum of the right-hand side of (37), the thesis ensues. □

We remark that the present proof is easily generalizable to the case in which ε and μ are not uniform scalars in Ω_r.

Appendix B
Analytical Solution for Lossy Waveguide

Since a time simulation includes transients, we extend the known frequency-domain solution of the lossless case [22] to the whole complex plane by substituting $j\omega \to s$, with s the complex variable. We derive an analytical form for the transverse electric field component $\mathrm{E_y}(\mathbf{r}, t) = \mathcal{L}^{-1}\{\mathcal{E}_y(\mathbf{r}, s)\}(t)$ in the time domain, with boundary conditions

$$\begin{cases} \mathcal{E}_y(\mathbf{r}, s) = \sin\left(\dfrac{\pi x}{a}\right) \mathcal{H}(s), & z = 0 \\ \mathcal{E}_y(\mathbf{r}, s) = 0, & z = \ell \end{cases}$$

where a is the size of the waveguide in the x-direction, ℓ is the distance in the longitudinal direction z at which the PEC wall is applied, and $\mathcal{H}(s)$ is the Laplace transform of the function $h(t)$ modulating the incident field. By plugging the boundary conditions, we get

$$\mathcal{E}_y(\mathbf{r}, s) = \sin\left(\frac{\pi x}{a}\right) \mathcal{H}(s) \left(\frac{e^{-\Gamma(s)\left(\frac{z-\ell}{c}\right)} - e^{\Gamma(s)\left(\frac{z-\ell}{c}\right)}}{e^{\Gamma(s)\frac{\ell}{c}} - e^{-\Gamma(s)\frac{\ell}{c}}} \right) \tag{38}$$

where $\Gamma(s) = \sqrt{s^2 + (c\pi/a)^2}$ and $c = 1/\sqrt{\mu\varepsilon}$ is the speed of light. (38) can be rewritten as

$$\begin{aligned} &\mathcal{E}_y(\mathbf{r}, s) \\ &= \sin\left(\frac{\pi x}{a}\right) \mathcal{H}(s) \left(\frac{e^{-\Gamma(s)\frac{z}{c}} - e^{\Gamma(s)\left(\frac{z-2\ell}{c}\right)}}{1 - e^{-2\Gamma(s)\frac{\ell}{c}}} \right) \\ &= \sin\left(\frac{\pi x}{a}\right) \mathcal{H}(s) \left(e^{-\Gamma(s)\frac{z}{c}} - e^{\Gamma(s)\left(\frac{z-2\ell}{c}\right)} \right) \sum_{n=0}^{+\infty} e^{-\Gamma(s)\left(\frac{2n\ell}{c}\right)} \\ &= \sin\left(\frac{\pi x}{a}\right) \mathcal{H}(s) \left(\sum_{n=0}^{+\infty} e^{-\Gamma(s)\left(\frac{z+2n\ell}{c}\right)} - \sum_{n=1}^{+\infty} e^{\Gamma(s)\left(\frac{z-2n\ell}{c}\right)} \right) \end{aligned}$$

where we have used the fact that $|e^{-2\Gamma(s)(\ell/c)}| \leq 1$, which stems from the fact that $\mathrm{Re}\{\Gamma(s)\} \geq 0$. From the linearity of both the inverse Laplace transform and the convolution integral, it ensues

$$\begin{aligned} \mathrm{E_y}(\mathbf{r}, t) = \mathcal{L}^{-1}\{\mathcal{E}_y(\mathbf{r}, s)\}(t) &= \sin\left(\frac{\pi x}{a}\right) \\ &\times \left(\sum_{n=0}^{+\infty} h * \mathcal{L}^{-1}\left\{ e^{-\Gamma(s)\left(\frac{z+2n\ell}{c}\right)} \right\}(t) + \right. \\ &\left. - \sum_{n=1}^{+\infty} h * \mathcal{L}^{-1}\left\{ e^{\Gamma(s)\left(\frac{z-2n\ell}{c}\right)} \right\}(t) \right). \end{aligned} \tag{39}$$

From [23, eq. (29.3.95)], for any real nonnegative number k, it straightforwardly follows that:

$$\begin{aligned} \mathcal{L}^{-1}\{e^{-k\Gamma(s)}\}(t) &= \mathcal{L}^{-1}\left\{ e^{-k\sqrt{s^2 + \left(\frac{c\pi}{a}\right)^2}} \right\}(t) \\ &= \delta(t-k) - \frac{c\pi}{a} k \frac{J_1\left(\frac{c\pi}{a}\sqrt{t^2 - k^2}\right)}{\sqrt{t^2 - k^2}} \Theta(t-k) \end{aligned} \tag{40}$$

where $\delta(t)$ is the Dirac delta distribution and $J_1(\alpha)$ is the first cylindrical Bessel function. We remark that k must be nonnegative for the Laplace transform to be well defined. This is always the case in (39), since in each term of the first series, $k = (z + 2n\ell)/c \geq 0$ and in each term of the second series, $k = (2n\ell - z)/c \geq 0$ (since the sum starts from $n = 1$). To extend this result to the case of a conductive medium filling the waveguide, it suffices to notice that in this case, we can define an equivalent permittivity $\varepsilon' = \varepsilon + \sigma/s$ and by substituting it into $\Gamma(s)$ (and in the speed of light), we find that

$$\mathcal{L}^{-1}\left\{ e^{-k\Gamma(s)} \right\}(t) = \left\{ \begin{array}{ll} g_1(t), & \text{for } \sigma \leq \dfrac{2\pi}{a}\sqrt{\dfrac{\varepsilon}{\mu}} \\ \\ g_2(t), & \text{for } \sigma \geq \dfrac{2\pi}{a}\sqrt{\dfrac{\varepsilon}{\mu}} \end{array} \right\}$$

where we have further defined

$$g_1(t) = e^{-\xi t}\left[\delta(t-k) - \alpha k \frac{J_1(\alpha\sqrt{t^2 - k^2})}{\sqrt{t^2 - k^2}} \Theta(t-k) \right]$$

$$g_2(t) = e^{-\xi t}\left[\delta(t-k) + \alpha k \frac{I_1(\alpha\sqrt{t^2 - k^2})}{\sqrt{t^2 - k^2}} \Theta(t-k) \right]$$

$$\xi = \frac{\sigma}{2\varepsilon}, \quad \alpha = \sqrt{\left| \left(\frac{c\pi}{a}\right)^2 - \xi^2 \right|}.$$

Here, $I_1(t)$ denotes the first modified cylindrical Bessel function. It is readily shown that, in the case $\sigma = 0$, we retrieve (40). The closed forms of other nonzero components of the electromagnetic field can be found with analogous steps.

Acknowledgment

The authors would like to thank the anonymous reviewers for their comments and questions which greatly improved the quality of this paper.

REFERENCES

[1] K. S. Yee, "Numerical solution of initial boundary value problems involving Maxwell's equations in isotropic media," *IEEE Trans. Antennas Propag.*, vol. AP-14, no. 3, pp. 302–307, May 1966.

[2] A. Taflove and S. Hagness, *Computational Electrodynamics: The Finite Difference Time Domain Method*, 2nd ed. Boston MA, USA: Artech House, 2000.

[3] T. Weiland, "Time domain electromagnetic field computation with finite difference methods," *Int. J. Numer. Model., Electron. Netw., Devices Fields*, vol. 9, no. 4, pp. 295–319, Jul. 1996.

[4] G. R. Werner and J. R. Cary, "A stable FDTD algorithm for non-diagonal, anisotropic dielectrics," *J. Comput. Phys.*, vol. 226, no. 1, pp. 1085–1101, Sep. 2007.

[5] A. F. Oskooi, C. Kottke, and S. G. Johnson, "Accurate finite-difference time-domain simulation of anisotropic media by subpixel smoothing," *Opt. Lett.*, vol. 34, no. 18, pp. 2778–2780, Sep. 2009.

[6] J.-F. Lee, R. Lee, and A. Cangellaris, "Time-domain finite-element methods," *IEEE Trans. Antennas Propag.*, vol. 45, no. 3, pp. 430–442, Mar. 1997.

[7] J. M. Jin, *The Finite Element Method in Electromagnetics*, 2nd ed. New York, NY, USA: Wiley, 2002.

[8] J. Kim and F. L. Teixeira, "Parallel and explicit finite-element time-domain method for Maxwell's equations," *IEEE Trans. Antennas Propag.*, vol. 59, no. 6, pp. 2350–2356, Jun. 2011.

[9] N. K. Madsen, "Divergence preserving discrete surface integral methods for Maxwell's curl equations using non-orthogonal unstructured grids," *J. Comput. Phys.*, vol. 119, no. 1, pp. 34–45, 1995.

[10] P. Alotto, A. De Cian, and G. Molinari, "A time-domain 3-D full-Maxwell solver based on the cell method," *IEEE Trans. Magn.*, vol. 42, no. 4, pp. 799–802, Apr. 2006.

[11] M. Cinalli and A. Schiavoni, "A stable and consistent generalization of the FDTD technique to nonorthogonal unstructured grids," *IEEE Trans. Antennas Propag.*, vol. 54, no. 5, pp. 1503–1512, May 2006.

[12] M. Marrone and R. Mittra, "A new stable hybrid three-dimensional generalized finite difference time domain algorithm for analyzing complex structures," *IEEE Trans. Antennas Propag.*, vol. 53, no. 5, pp. 1729–1737, May 2005.

[13] L. Codecasa and M. Politi, "Explicit, consistent, and conditionally stable extension of FD-TD to tetrahedral grids by FIT," *IEEE Trans. Magn.*, vol. 44, no. 6, pp. 1258–1261, Jun. 2008.

[14] L. Codecasa, R. Specogna, and F. Trevisan, "A new set of basis functions for the discrete geometric approach," *J. Comput. Phys.*, vol. 229, no. 19, pp. 7401–7410, 2010.

[15] M. Cicuttin, L. Codecasa, B. Kapidani, R. Specogna, and F. Trevisan, "GPU accelerated time-domain discrete geometric approach method for Maxwell's equations on tetrahedral grids," *IEEE Trans. Magn.*, vol. 54, no. 3, Mar. 2018, Art. no. 7203004.

[16] S. Dosopoulos and J.-F. Lee, "Interior penalty discontinuous Galerkin finite element method for the time-dependent first order Maxwell's equations," *Antennas Propag.*, vol. 58, no. 12, pp. 4085–4090, 2010.

[17] S. D. Gedney, J. C. Young, T. C. Kramer, and J. A. Roden, "A discontinuous Galerkin finite element time-domain method modeling of dispersive media," *IEEE Trans. Antennas Propag.*, vol. 60, no. 4, pp. 1969–1977, Apr. 2012.

[18] F. Edelvik, R. Schuhmann, and T. Weiland, "A general stability analysis of FIT/FDTD applied to lossy dielectrics and lumped elements," *Int. J. Numer. Model.*, vol. 17, no. 4, pp. 407–419, 2004.

[19] M. Marrone and R. Mittra, "A theoretical study of the stability criteria for hybridized FDTD algorithms for multiscale analysis," *IEEE Trans. Antennas Propag.*, vol. 52, no. 8, pp. 2158–2167, Aug. 2004.

[20] P. Monk and E. Süli, "A convergence analysis of Yee's scheme on nonuniform grids," *SIAM J. Numer. Anal.*, vol. 31, no. 2, pp. 393–412, 1994.

[21] B. Krietenstein, R. Schuhmann, P. Thoma, and T. Weiland, "The perfect boundary approximation technique facing the big challenge of high precision field computation," in *Proc. 19th Int. LINAC Conf.*, Chicago, IL, USA, Aug. 1998, pp. 860–862.

[22] R. E. Collin, *Foundations for Microwave Engineering*, 2nd ed. New York, NY, USA: McGraw-Hill, 1992, pp. 190–192.

[23] M. Abramowitz and I. Stegun, *Handbook of Mathematical Functions*. New York, NY, USA: Dover, 1965, p. 1027.

Lorenzo Codecasa (M'08) received the Laurea degree (Hons.) and the Ph.D. degree in electronic engineering from the Politecnico di Milano, Milan, Italy, in 1997 and 2001, respectively.

From 2002 to 2010, he was an Assistant Professor of electrical engineering with the Department of Electronics, Information, and Bioengineering, Politecnico di Milano, where he has been an Associate Professor of electrical engineering since 2010. His current research interests include the theoretical analysis and the computational investigation of electric circuits and electromagnetic fields. In his research areas, he has authored or co-authored over 180 papers in refereed international journals and conference proceedings.

Dr. Codecasa received the 2015 Harvey Rosten Award of Excellence for his contributions in electrothermal modeling of electronic circuits.

Bernard Kapidani received the M.Sc. degree in electronic engineering and the Ph.D. degree *(cum laude)* in electrical engineering from the University of Udine, Udine, Italy, in 2014 and 2018, respectively.

He is currently a Post-Doctoral Researcher with the Institute for Analysis and Scientific Computing, Technical University of Vienna, Vienna, Austria. His current research interests include time-domain methods for the numerical solution of Maxwell's equations and the application of computational mathematics to computational electromagnetism.

Ruben Specogna (S'05–M'08) received the M.Sc. degree in electronic engineering and the Ph.D. degree in electrical engineering from the University of Udine, Udine, Italy, in 2003 and 2007, respectively.

He was an Assistant Professor with the University of Udine from 2008 to 2016, where he has been an Associate Professor since 2016. He has authored over 90 papers in international scientific journals, in the field of computational electromagnetism, coupled problems, computational topology and computer-aided design, nuclear fusion reactors engineering and design, and lab-on-a-chip biosensors.

Francesco Trevisan was born in Treviso, Italy, in 1964. He received the Degree (Hons.) in ingegneria elettrotecnica (power electrical engineering) from the University of Padova, Padua, Italy, in 1988.

Since 1991, he has been a Researcher with the Magnet System Group, Istituto Gas Ionizzati, National Research Council, Padua, where he has been involved in the electromagnetic design of the experimental machine reverse field experiment for research on magnetically confined nuclear fusion. Since 1995, he has also been an Associate Professor with the Polytechnic Department of Engineering and Architecture, University of Udine, Udine, Italy. His current research interests include discrete geometric formulations for the computation of electric and magnetic fields and on the methodologies for solving inverse problems in electromagnetics. He has authored or co-authored over 120 scientific papers on computational electromagnetics. He is involved in international research projects in the area.

Mr. Trevisan has been a member of the Editorial Board of the COMPUMAG, an international conference on computational electromagnetism.